

Optical conductivity of granular aluminum films near the metal to insulator transition: evidence for a BCS-BEC crossover

Aviv Glezer Moshe,^{1,2} Eli Farber,² and Guy Deutscher¹

¹*Raymond and Beverly Sackler School of Physics and Astronomy, Tel Aviv University, Tel Aviv, Israel*

²*Department of Physics and Department of Electrical and Electronic Engineering, Ariel University, P.O.B. 3, Ariel 40700, Israel.*

(Dated: May 20, 2022)

We report measurements of the energy gap of granular aluminum films by THz spectroscopy. We find that as the grains progressively decouple, the coupling ratio $2\Delta(0)/k_B T_c$ increases above the BCS weak coupling ratio 3.53, and reaches a values consistent with a BCS-BEC crossover for the high resistivity samples. The Mattis-Bardeen (MB) formalism describes remarkably well the behavior of $\sigma_{1,s}/\sigma_{1,n}$ for all samples up to very high normal state resistivities.

INTRODUCTION

In view of their possible applications as high kinetic inductance elements in quantum circuits (QC), there has been recently renewed interest in the properties of strongly disordered superconductors in the vicinity of the metal to insulator (M/I) transition. The optical properties of disordered NbN films have been the focus of particular attention [1, 2]. It was found that in these films, where disorder has a homogeneous distribution on the atomic scale, the coupling ratio $2\Delta(0)/k_B T_c$ decreases continuously below the weak coupling limit value 3.53 when disorder is increased. This decrease becomes very pronounced when the parameter $k_F l$, where k_F is the Fermi wave vector and l the electron mean free path, becomes of order unity [1]. At the highest resistivity investigated ($\sim 1,000 \mu\Omega cm$) there is not even a clear optical gap edge. At the same time the coupling ratio obtained from the tunneling gap remains at about 4.2. This behavior departs from the predictions of the BCS Mattis-Bardeen theory [3]. The enhanced low frequency dissipation has detrimental consequences on the quality factor of high impedance resonators that could be used in QC [4].

On the other hand larger optical gap values have been reported for high resistivity granular Al films [5] as well as lower dissipation values [4]. Whether the optical behavior is universal for all kinds of disorder is therefore an open question that has not so far been examined in depth. In this work we present a detailed study of the optical properties of granular Al thin films, where disorder is on the grain size scale (about 2 nm [6]) rather than on the atomic scale. We find that up to near the metal to insulator transition the optical gap edge remains well defined and that, contrary to the behavior of disordered NbN films, the ratio $2\Delta(0)/k_B T_c$ increases as the resistivity increases, reaching a value of 4.51 in the highest resistivity sample ($\sim 8,000 \mu\Omega cm$) studied. This behavior is favorable for QC applications. In light of the recent work of Pisani et al. [7, 8], we interpret the increase of the coupling ratio as indicating an approach to a BCS to Bose-Einstein condensate (BEC) crossover, occurring near the Mott metal to insulator transition triggered by the electrostatic charging energy of the grains [9]. The highest resistivity sample is not far from the unitary limit and the value of the coupling ratio is consistent

with the experimental value of the coherence length. We propose that the difference in behavior between NbN and granular Al films stems from the different nature of the metal to insulator transition, being of the Anderson type in the former [10] and of the Mott type in the latter [11].

EXPERIMENTAL AND METHODS

Granular aluminum thin films were prepared by thermal evaporation of clean Al pellets in a controlled O_2 pressure, where the base pressure of the vacuum chamber is $\sim 1 \times 10^{-7}$ Torr. The films were deposited onto liquid nitrogen cooled substrates ($10 \times 10 \times 2 mm^3$ MgO or $10 \times 10 \times 1 mm^3$ LSAT, which result in similar fabry-perot pattern in the optical spectra). Films with various degree of grain coupling were obtained by varying the O_2 partial pressure in the range of $2 - 5 \times 10^{-5}$ Torr while keeping the deposition rate about $5 \pm 1 \text{ \AA/s}$, similar to previous work [5, 12]. The films thickness varied in the range $40 - 100 nm$ in order to obtain high quality transmission measurements as the resistivity of the films increases.

Standard four point resistivity measurements were performed in either a commercial QD PPMS or in a home built probe, we characterize each film by its normal state resistivity ρ_n at 4.2 K. Great care was taken to obtain homogeneous films. Sharp superconducting transitions were obtained even for the highest resistivity films, see Fig. 2 in supplemental material.

The optical spectroscopy measurements were done by utilizing a quasi-optical Mach-Zehnder interferometer which allows us to obtain the complex transmission $\hat{t} = |t| e^{i\phi_t}$ [5, 13] of the substrate-film system. The radiation sources are tunable monochromatic backward-wave oscillators (BWO), by utilizing several sources we cover a frequency range of $3 - 17 cm^{-1}$ (or about $0.1 - 0.5$ THz). Commercial optical 4He cryostat with a home built sample holder, provides us dynamic temperature range down to $1.5 K$ and the ability to measure up to two samples during one cooldown. The complex transmission was measured for all samples at 4.2 K and at various temperatures close to and below T_c down to $1.5 K$. Then the complex conductivity $\hat{\sigma}(\omega) = \sigma_1(\omega) + i\sigma_2(\omega)$ is calculated from

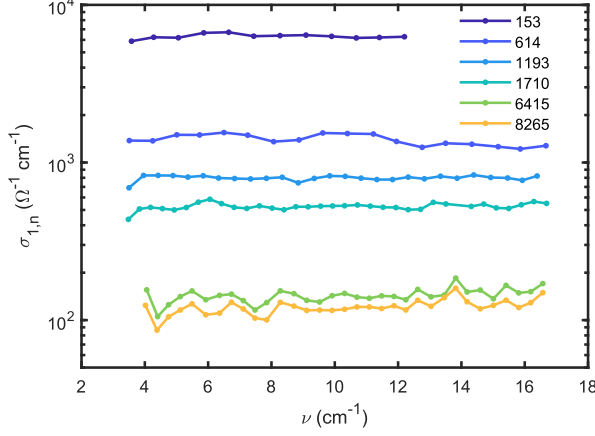


Figure 1. Real part of the optical conductivity at 4.2 K for all samples. The legend marks the normal state resistivity in $\mu\Omega cm$ as obtained from transport measurements of the same samples.

the measured complex transmission via the Fresnel equations [13, 14], without relying on any microscopic model.

RESULTS

To allow an easy comparison with the behavior of NbN films [1, 2] our main results are displayed Table I. To evaluate $k_F l$ we approximate it by the free electron formula $k_F l = \frac{m}{\hbar} \frac{1}{\rho} v_F \rho l$ by using the values of $v_F = 15.99 \times 10^7 cm/s$ and $\rho l = 5.01 \times 10^{-6} \mu\Omega cm^2$ as obtained by Gall [15] for clean aluminum. For all samples, except for sample 1, the value of $k_F l$ is equal to or smaller than one, in sharp contrast with the behavior of the studied NbN films [1, 2].

Sample ID	$\rho_{4.2K}^n (\mu\Omega cm)$	$k_F l$	T_c (K)	$2\Delta(0)/k_B T_c$
1	153	4.38	3.08	3.56
2	614	1.00	2.95	3.64
3	1193	0.55	2.71	3.73
4	1710	0.36	2.60	3.77
5	6415	0.10	2.26	4.29
6	8265	0.085	2.14	4.51

Table I. Studied samples properties.

The normal state conductivity $\sigma_{1,n}$ as measured at 4.2 K is frequency independent up to $17 cm^{-1}$, see Fig. 1. In the superconducting state a good fit to the MB theory [3] is obtained for all samples up to resistivities of about $8,000 \mu\Omega cm$, as one can see for two representative samples in Fig. 2. Values of $\Delta(0)$ used in table I were obtained from these fits. The complete data set can be found in Fig. 4, supplemental material. Up to the highest resistivity samples the superconducting transition is well defined, see Fig. 3.

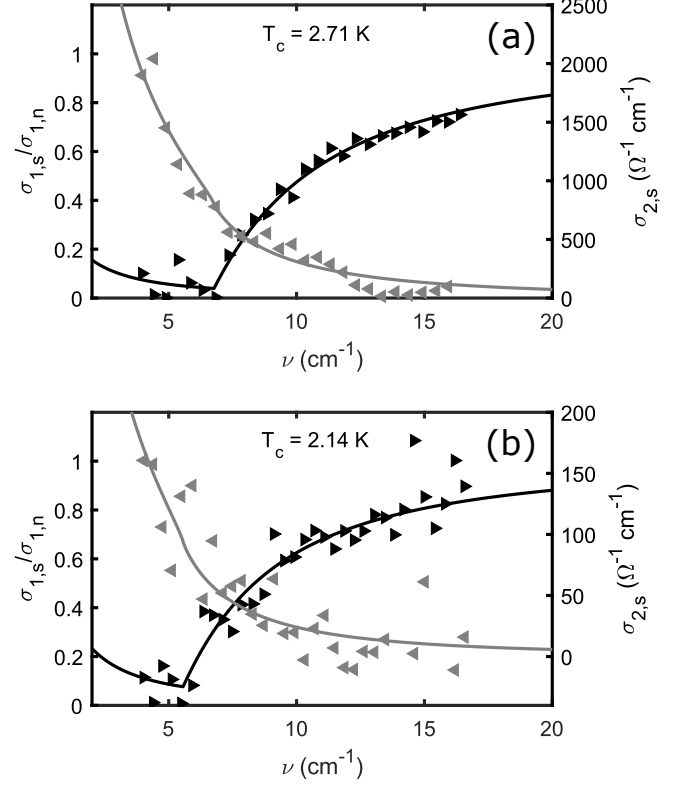


Figure 2. Optical conductivity $\hat{\sigma}(\omega)$ of (a) sample 3 and (b) sample 6 at $T = 1.5 K$. The black triangles and line are the normalized real part of the conductivity along its MB fit, the grey triangles and line are the imaginary part of the conductivity along its MB fit.

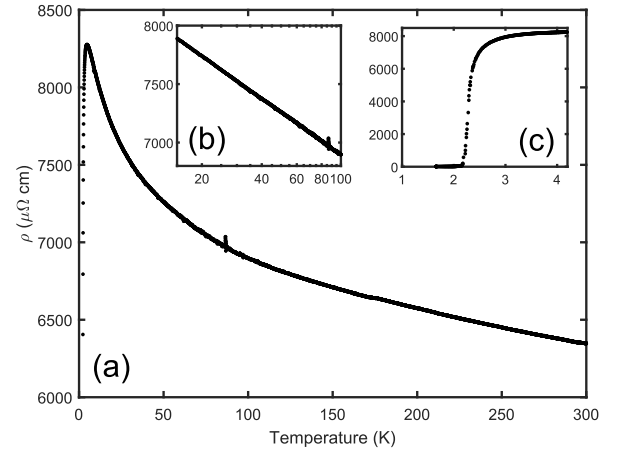


Figure 3. (a) Resistivity as a function of temperature of sample 6. Insets (b-c) are the same data focused on different temperatures scales: (b) The temperature is presented in a logarithmic scale, which shows logarithmic increase of ρ over wide range of temperatures. (c) The resistive SC transition.

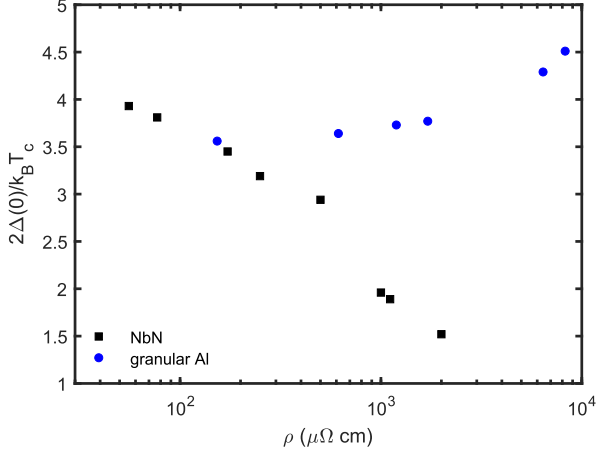


Figure 4. Coupling ratio versus resistivity. Black squares are NbN data from Ref. [1] and blue circles are our granular Al data.

DISCUSSION

First of all we compare our results to tunneling data. The value of the optical gap as determined from fitting the conductivity data to the MB theory is close to the value of the tunneling gap reported by Abeles and Hanak [16], up to and including the highest resistivity samples. According to them, the coupling ratio $2\Delta(0)/k_B T_c$ is equal to 3.4 for all specimen within 2%. In fact, according to the optical gap values reported in Table. 1, the coupling ratio increases continuously with resistivity, a trend already noted by Pracht et al. [5] for a high resistivity sample. This deviation appears to be systematic, the coupling ratio varying from 3.56 for the lowest resistivity sample (close to the weak coupling value of 3.53) up to 4.51 for the highest resistivity one. This is one of our main findings.

Second of all, we compare our results with those obtained by Cheng et al. on disordered NbN films [1]. As can be seen in Fig. 4, as the resistivity and $(k_F l)^{-1}$ increases, the coupling ratio *decreases* continuously, rather than increasing. Furthermore, the value of the optical gap becomes distinct from and smaller than the tunneling gap. At the highest resistivity investigated ($\sim 1,000 \mu\Omega \text{ cm}$) there is not even a clear optical gap edge. This difference in behavior between the optical data obtained on granular Al and NbN is emphasized in Fig. 5, where $\hbar\omega$ has been scaled by twice the value of the tunneling gap. While for granular Al the conductivities scale fairly, they clearly don't for NbN. These points deserve a detailed discussion.

Regarding the first one, the increase of the coupling ratio seen in granular Al with resistivity may have two different origins. The first one would be a stronger coupling to soft phonons often cited as the possible reason for the higher T_c of granular films [17]. However, we discard this interpretation here since the critical temperature is decreasing in our series of high resistivity samples. A second origin would be

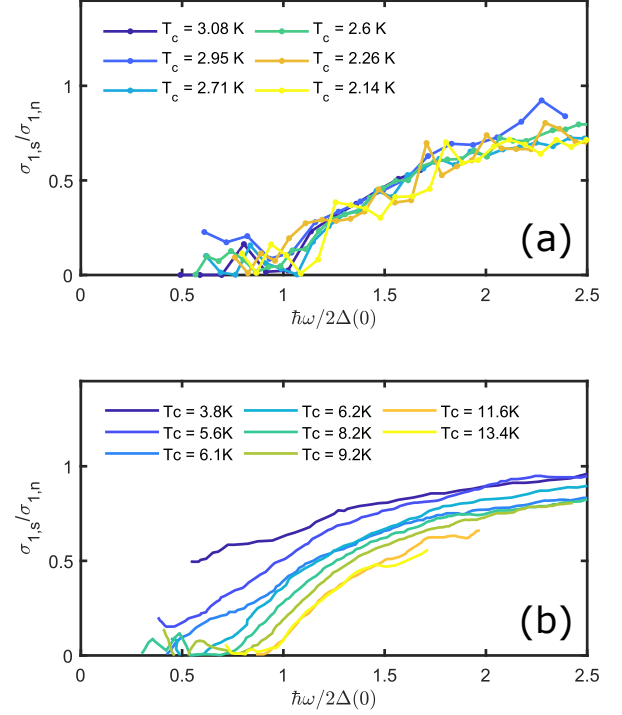


Figure 5. Real part of the optical conductivity, measured at the lowest temperature, normalized to the normal state conductivity. The frequency axis is normalized to twice the value of the tunneling gap. (a) our granular Al data (b) Cheng et al. NbN data [1].

an approach to a BCS to BEC crossover. In the case of a BE condensation, the pair breaking energy becomes disconnected from the $k_B T_c$ energy scale, which is much smaller. In the crossover regime from BCS to BE condensation the coupling ratio becomes progressively larger than the weak coupling limit value. We favor this second interpretation. This effect has been studied recently in detail by Pisani et al. [7, 8] who have calculated how T_c and the zero temperature gap $\Delta(0)$ vary with the distance to the unitary limit, where the product of the Fermi wave vector k_F by the scattering length a_F goes to infinity. When the coupling ratio reaches the value of 4.51, as is the case for our highest resistivity sample, $(k_F a)^{-1} \simeq -0.70$, not far from the unitary limit. Here the approach to BE condensation is due to confinement rather than to an increase in coupling strength, the cross-over taking place when the superconducting coherence length becomes of the same order as the grain size. In the highest resistivity sample it is in fact two to three times the grain size.

Concerning the second point, one can understand the difference in behavior between granular Al and disordered NbN films as resulting from their different disorder length scales, being respectively the grain size in granular Al and the lattice parameter or inter-atomic distance in NbN. In a 3D system the metal to insulator transition occurs when the conductiv-

ity g measured at the relevant length scale crosses a critical value g_c . Here g is the universal conductance $\frac{2e^2}{h}$ divided by the relevant length scale d . Since the grain size in granular Al is about one order of magnitude larger than the interatomic distance in NbN, it follows that the value of the critical conductivity in the former is expected to be about one order of magnitude larger than in the latter. However this argument does not explain the qualitative difference between the behaviors of the optical conductivities of granular Al and NbN seen in Fig. 5. As the M/I transition is approached a sharp gap edge persists in granular Al but not in NbN. This suggests that the nature of the M/I transition is not the same in the two systems. While it is of the Anderson type in NbN, we believe that it is of the Mott type in granular Al, as already proposed [11]. This is consistent with the large value of the coupling ratio, since at a Mott transition the effective bandwidth reduces to zero (while the DOS at the Fermi level remains finite [18]). As the bandwidth reduces the coupling ratio increases for any finite value of the gap. In DMFT models the ratio of the Coulomb energy to the bandwidth is close to 3 when the transition occurs [18]. In the granular case the value of the Coulomb energy is that of the electrostatic energy of the grains, which for a 2 nm size grain is about 30 meV [9]. An effective bandwidth of 10 meV is compatible with the value of 2.5 meV for the Fermi energy deduced from the value of the strong coupling ratio (see supplemental material). We note that the energy level splitting is also about 10 meV. We may add that the coherence length in NbN is always much larger than the disorder length scale, so that the system never approaches the BCS to BEC crossover and therefore never develops the strong coupling effect predicted by Pisani et al. [7, 8].

CONCLUSION

Optical spectroscopy reveals that a sharp gap edge persists in granular Aluminum films as the metallic grains are being decoupled towards the Metal to Insulator transition. Remarkably, at the same time the coupling ratio $2\Delta(0)/k_B T_c$ increases, reaching in the most resistive sample a value consistent with a proximity to the unitary limit. The critical temperature is not strongly reduced by the grain decoupling. This behavior is consistent with a Mott transition driven by the electrostatic charging energy of the grains.

This behavior is in contrast with that observed previously in atomically disordered NbN film, where the coupling ratio reduces when disorder is increased, the critical temperature goes down strongly and the sharp gap edge vanishes, a behavior consistent with an Anderson transition [10]. The origin of the good performance of high kinetic inductance granular Al resonators reported recently [4] may be due to the fact that the M/I transition is of the Mott type rather than of the Anderson

type. This granular system may indeed be viewed as a network of Josephson junctions between well-defined Al grains as suggested by Grunhaupt et al. [4], rather than as a highly disordered superconductor.

ACKNOWLEDGEMENTS

We acknowledge G. C. Strinati for fruitful discussion and for supplying us with Fig. 6 data in supplemental material. We are grateful to N. Bachar for guidance with early sample preparation and THz measurements.

* avivmoshe@mail.tau.ac.il

-
- [1] B. Cheng, L. Wu, N. J. Laurita, H. Singh, M. Chand, P. Raychaudhuri, and N. P. Armitage, Phys. Rev. B **93**, 180511 (2016).
 - [2] D. Sherman, U. S. Pracht, B. Gorshunov, S. Poran, J. Jesudasan, M. Chand, P. Raychaudhuri, M. Swanson, N. Trivedi, A. Auerbach, M. Scheffler, A. Frydman, and M. Dressel, Nature Physics **11**, 188 (2015).
 - [3] D. C. Mattis and J. Bardeen, Phys. Rev. **111**, 412 (1958).
 - [4] L. Grunhaupt, N. Maleeva, S. T. Skacel, M. Calvo, F. Levy-Bertrand, A. V. Ustinov, H. Rotzinger, A. Monfardini, G. Catealani, and I. M. Pop, Phys. Rev. Lett. **121**, 117001 (2018).
 - [5] U. S. Pracht, N. Bachar, L. Benfatto, G. Deutscher, E. Farber, M. Dressel, and M. Scheffler, Physical Review B **93**, 100503 (2016).
 - [6] G. Deutscher, M. Gershenson, E. GrÅEnbaum, and Y. Imry, Journal of Vacuum Science and Technology **10**, 697 (1973).
 - [7] L. Pisani, P. Pieri, and G. C. Strinati, Phys. Rev. B **98**, 104507 (2018).
 - [8] L. Pisani, A. Perali, P. Pieri, and G. C. Strinati, Phys. Rev. B **97**, 014528 (2018).
 - [9] B. Abeles, Physical Review B **15**, 2828 (1977).
 - [10] M. Mondal, A. Kamlapure, M. Chand, G. Saraswat, S. Kumar, J. Jesudasan, L. Benfatto, V. Tripathi, and P. Raychaudhuri, Phys. Rev. Lett. **106**, 047001 (2011).
 - [11] N. Bachar, S. Lerer, A. Levy, S. Hacohe-Gourgy, B. Almog, H. Saadaoui, Z. Salman, E. Morenzoni, and G. Deutscher, Physical Review B **91**, 041123 (2015).
 - [12] N. Bachar, U. Pracht, E. Farber, M. Dressel, G. Deutscher, and M. Scheffler, Journal of Low Temperature Physics **179**, 83 (2015).
 - [13] U. S. Pracht, E. Heintze, C. Clauss, D. Hafner, R. Bek, D. Werner, S. Gelhorn, M. Scheffler, M. Dressel, D. Sherman, B. Gorshunov, K. S. Il'in, D. Henrich, and M. Siegel, IEEE Transactions on Terahertz Science and Technology **3**, 269 (2013).
 - [14] M. Dressel and G. Gruner, eds., *Electrodynamics of Solids* (Cambridge University Press, 2002).
 - [15] D. Gall, Journal of Applied Physics **119**, 085101 (2016), <https://doi.org/10.1063/1.4942216>.
 - [16] B. Abeles and J. Hanak, Physics Letters A **34**, 165 (1971).
 - [17] J. W. Garland, K. H. Bennemann, and F. M. Mueller, Phys. Rev. Lett. **21**, 1315 (1968).
 - [18] A. Georges, G. Kotliar, W. Krauth, and M. J. Rozenberg, Rev. Mod. Phys. **68**, 13 (1996).

Supplemental material for: Optical conductivity of granular aluminum films near the metal to insulator transition: evidence for a BCS-BEC crossover

Aviv Glezer Moshe,^{1,2} Eli Farber,² and Guy Deutscher¹

¹Raymond and Beverly Sackler School of Physics and Astronomy, Tel Aviv University, Tel Aviv, Israel

²Department of Physics and Department of Electrical and Electronic Engineering, Ariel University, P.O.B. 3, Ariel 40700, Israel.

(Dated: May 20, 2022)

I. TRANSPORT PROPERTIES

Fig. 1 shows the superconducting (SC) critical temperature as a function of the normal state resistivity at 4.2 K for films studied in this work and also that of Hall bars prepared separately in our lab. The well known “dome” shaped phase diagram [1–4] can be clearly seen. The resistive SC transition for all studied samples, along with their measured SC gap $\Delta(T)$ as a function of reduced temperature T/T_c is presented in Fig. 2, where we define T_c as the temperature where the resistivity has decreased below 1% of its normal state value.

II. OPTICAL CONDUCTIVITY DATA ANALYSIS

In figures 3 and 4 the frequency ν is given in units of cm^{-1} which is related to ω by $\omega = 2\pi c\nu$, where c is the speed of light in cm/sec . We analyze the optical data similarly to the method used by Pracht et al. [4]. Representative transmission $|t|^2$ and frequency normalized phase spectra ϕ/ν are shown in Fig. 3, for both normal (at 4.2 K) and superconducting state. The strong oscillation pattern is due to multiple reflections inside the substrate. Utilizing the Fresnel equations for multiple reflections in a bilayer system [5–7], we obtain the complex conductivity $\hat{\sigma}(\omega) = \sigma_1(\omega) + i\sigma_2(\omega)$, without relying on any microscopic model. The measured transmission depends on both the substrate and film dielectric function $\hat{\epsilon}(\omega)$ and thickness

$$\hat{t} = t(d_s, \epsilon_1^s(\omega), \epsilon_2^s(\omega); d_f, \epsilon_1^f(\omega), \epsilon_2^f(\omega)) \quad (1)$$

where $\hat{\epsilon}(\omega) = \epsilon_1(\omega) + i\epsilon_2(\omega)$ which can be expressed as complex conductivity $\hat{\sigma}(\omega)$ by the relation

$$\hat{\epsilon}(\omega) = 1 + i \frac{2\pi}{\epsilon_0} \frac{\hat{\sigma}(\omega)}{\omega} \quad (2)$$

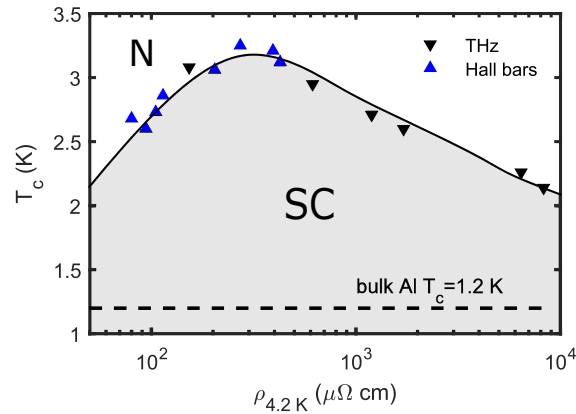


Figure 1. Critical temperature of studied granular aluminum films versus the normal state resistivity. Black upside down triangles (▼) marks T_c of the optical spectroscopy studied samples. Blue triangles (▲) marks T_c as measured by Hall bars with similar deposition conditions as described in the main text. The dashed line marks the bulk aluminum critical temperature.

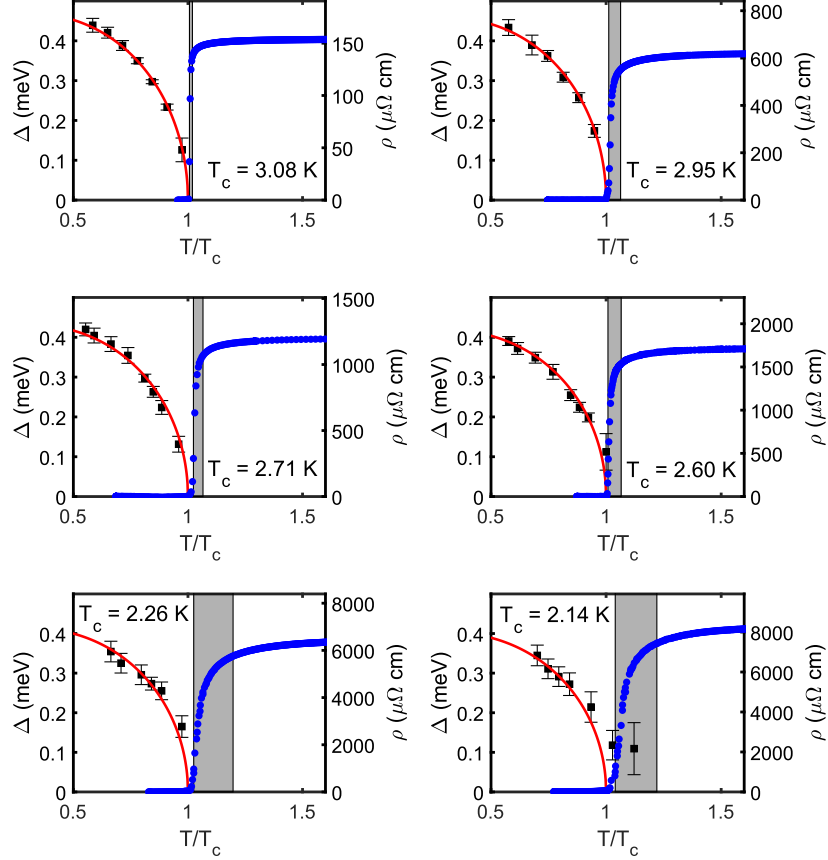


Figure 2. $\Delta(T)$ and $\rho(T)$ versus temperature for all studied samples. Black squares (■) are the measured gap, obtained by fitting $\sigma_{1,s}/\sigma_{1,n}$ to MB formulae and the red curve is a fit to a BCS gap equation curve. Blue circles (●) are the measured resistivity and the grey area marks the decrease of the normal state resistivity from 90 to 10% of its normal state value.

Once \hat{t} is measured, we need to disentangle the substrate contribution in order to extract the complex conductivity of the film. The MgO and LSAT dielectric substrates are known to be completely transparent (means $\epsilon_2^s = 0$) in the THz frequency range [4, 8], as we also checked in a separate experiment. We first analyze the normal state at 4.2 K, where the normal state conductivity obeys Drude model with high scattering rate relatively to the measured frequency range, in this low frequency regime $\sigma_2 \simeq 0$. We fit around each maxima/minima in the spectra with σ_1 of the film and ϵ_1 of the substrate. We then use the obtained set of ϵ_1 for the low temperature data where we fit around each maxima/minima by both σ_1 , σ_2 of the film. This process yields a pair of σ_1 , σ_2 for each frequency point, as can be shown in Fig. 3.

Once we obtain $\hat{\sigma}(\omega, T)$ we fit it to the Mattis-Bardeen (MB) formulas [9], which are appropriate since we are well in the dirty limit $\Delta \ll \hbar/\tau$ [4, 10, 11].

$$\begin{aligned}
 \frac{\sigma_1(\omega)}{\sigma_n} &= \frac{e^2 n_s}{m^* \sigma_n} \pi \delta(\omega) \\
 &+ \frac{2}{\hbar \omega} \int_{\Delta}^{\infty} dE g(E) [f(E) - f(E + \hbar \omega)] \\
 &- \frac{\Theta(\hbar \omega - 2\Delta)}{\hbar \omega} \int_{\Delta - \hbar \omega}^{-\Delta} dE g(E) [1 - 2f(E + \hbar \omega)]
 \end{aligned} \tag{3}$$

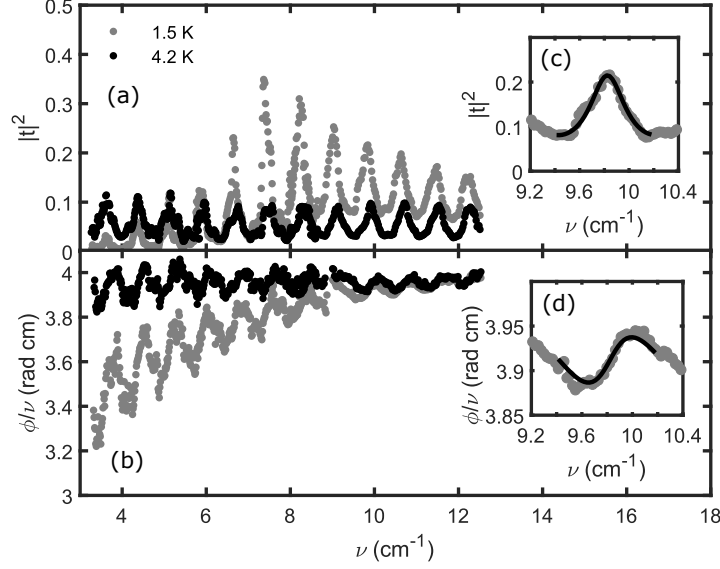


Figure 3. Raw data of sample 1. (a) Transmittance. (b) phase divided by frequency in the normal (black) and SC (grey) state. Figures (c) and (d) show an example of the resulting simultaneous fit to both $|t|^2$ and ϕ_t/ν (black line) by σ_1 , σ_2 of the film.

$$\frac{\sigma_2(\omega)}{\sigma_n} = \frac{1}{\hbar\omega} \int_{\max\{-\Delta, \Delta-\hbar\omega\}}^{\Delta} dE g(E) [1 - 2f(E + \hbar\omega)] \times \frac{E(E + \hbar\omega) + \Delta^2}{\sqrt{\Delta^2 - E^2} \sqrt{(E + \hbar\omega)^2 - \Delta^2}} \quad (4)$$

$$g(E) = \frac{E(E + \hbar\omega) + \Delta^2}{\sqrt{E^2 - \Delta^2} \sqrt{(E + \hbar\omega)^2 - \Delta^2}} \quad (5)$$

The normal state conductivity is determined as $\sigma_1(\omega)$ at 4.2 K, we then fit σ_1/σ_n with Δ as the sole fitting parameter. For some of the samples the behavior of $\sigma_1(\omega)$ at sub-gap frequencies $\omega < 2\Delta/\hbar$ slightly deviates from MB and therefore are being excluded from the fit. We then fit $\Delta(T)$ to the standard BCS gap equation [12] with $\Delta(0)$ as the sole fitting parameter, without any restriction on the coupling ratio $2\Delta(0)/k_B T_c$.

The complex conductivity for all samples at the lowest measured temperature along with its MB fit is shown in Fig. 4 with good agreement for all samples.

III. BCS-BEC CROSSOVER

Pisani et al. [13, 14] calculated the coupling ratio $\frac{2\Delta}{k_B T_c}$ versus $(k_F a_F)^{-1}$, where k_F is the Fermi wave vector and a_F is the s-wave scattering length. We note that it is possible to describe the crossover in terms of the variable $k_F \xi_{pair}$ [15], which has been calculated as a function of $(k_F a_F)^{-1}$ [16].

For our most resistive sample having a coupling ratio of 4.51 we obtain $k_F \xi_{pair} = 2.28$ or $(k_F a_F)^{-1} = -0.70$ which is not far from the unitary limit $(k_F a_F)^{-1} = 0$ (see Fig. 5). Pisani et al. [13] also calculated the value of $\Delta(0)/E_F$ as a function of the tunable parameter $(k_F a_F)^{-1}$. For a given coupling ratio as measured by us, we use it to evaluate E_F and therefore k_F (assuming that the effective mass is not too different than that of a bare electron). For our most resistive sample $\Delta(0)/E_F = 0.17$ which yields $E_F = 2.47 \text{ meV}$ and $k_F = 2.54 \times 10^8 \text{ m}^{-1}$. Upper critical field measurements of similar samples [17] yield a coherence length of about $\xi_0 \simeq 10 \text{ nm} \simeq \xi_{pair}$. we obtain $k_F \xi_{pair} = 2.54$, which is close to the value obtained by the coupling ratio alone.

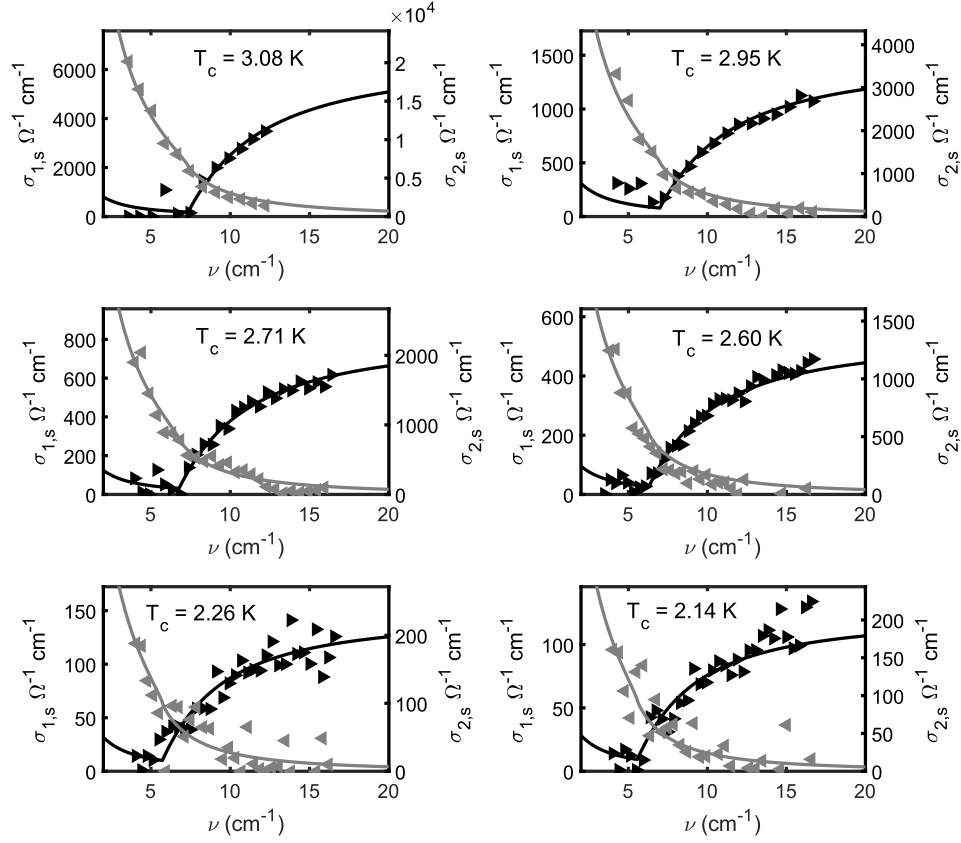


Figure 4. Optical conductivity $\hat{\sigma}(\omega)$ of all samples. The black triangles and line are the real part of the conductivity and its MB fit, the grey triangles and line are the imaginary part of the conductivity and its MB fit. The data is shown for $T = 1.5 K$, except for sample 2 ($T_c = 2.95 K$) which was measured down to $T = 1.7 K$.

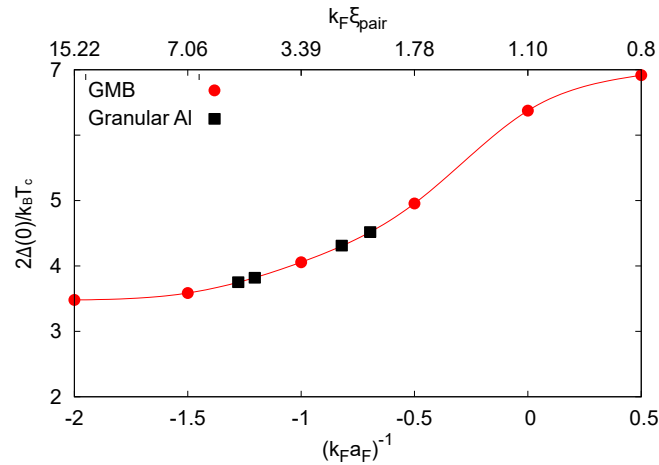


Figure 5. The coupling ratio as a function of $k_F \xi_{pair}$ or $(k_F a_F)^{-1}$ (Pisani et al., private communication). The red circles (●) are the results of the numerical calculations that include corrections beyond mean field which arise from pairing fluctuations, labeled GMB. The red line joining these circles is a guide to the eye. The black squares (■) correspond to our measured coupling ratio. The corresponding values of $(k_F a_F)^{-1}$ range from -1.3 to -0.7 and those of $k_F \xi_{pair}$ from 5.3 to 2.3.

* avivmoshe@mail.tau.ac.il

-
- [1] N. Bachar, S. Lerer, S. Hacohe-Gourgy, B. Almog, and G. Deutscher, *Physical Review B* **87**, 214512 (2013).
 - [2] G. Deutscher, M. Gershenson, E. Grunbaum, and Y. Imry, *Journal of Vacuum Science and Technology* **10**, 697 (1973).
 - [3] G. Deutscher, H. Fenichel, M. Gershenson, E. G. nbaum, and Z. Ovadyahu, *Journal of Low Temperature Physics* **10**, 231 (1973).
 - [4] U. S. Pracht, N. Bachar, L. Benfatto, G. Deutscher, E. Farber, M. Dressel, and M. Scheffler, *Physical Review B* **93**, 100503 (2016).
 - [5] B. Gorshunov, A. Volkov, I. Spektor, A. Prokhorov, A. Mukhin, M. Dressel, S. Uchida, and A. Loidl, *International Journal of Infrared and Millimeter Waves* **26**, 1217 (2005).
 - [6] U. S. Pracht, E. Heintze, C. Clauss, D. Hafner, R. Bek, D. Werner, S. Gelhorn, M. Scheffler, M. Dressel, D. Sherman, B. Gorshunov, K. S. Il'in, D. Henrich, and M. Siegel, *IEEE Transactions on Terahertz Science and Technology* **3**, 269 (2013).
 - [7] M. Dressel and G. Gruner, eds., *Electrodynamics of Solids* (Cambridge University Press, 2002).
 - [8] S. Arezoomandan, A. Prakash, A. Chanana, J. Yue, J. Mao, S. Blair, A. Nahata, B. Jalan, and B. Sensale-Rodriguez, *Scientific Reports* **8**, 3577 (2018).
 - [9] D. C. Mattis and J. Bardeen, *Phys. Rev.* **111**, 412 (1958).
 - [10] U. S. Pracht, T. Cea, N. Bachar, G. Deutscher, E. Farber, M. Dressel, M. Scheffler, C. Castellani, A. M. Garc a-Garc a, and L. Benfatto, *Physical Review B* **96**, 094514 (2017).
 - [11] N. Bachar, U. Pracht, E. Farber, M. Dressel, G. Deutscher, and M. Scheffler, *Journal of Low Temperature Physics* **179**, 83 (2015).
 - [12] J. Bardeen, L. N. Cooper, and J. R. Schrieffer, *Physical Review* **108**, 1175 (1957).
 - [13] L. Pisani, P. Pieri, and G. C. Strinati, *Phys. Rev. B* **98**, 104507 (2018).
 - [14] L. Pisani, A. Perali, P. Pieri, and G. C. Strinati, *Phys. Rev. B* **97**, 014528 (2018).
 - [15] F. Pistolesi and G. C. Strinati, *Phys. Rev. B* **49**, 6356 (1994).
 - [16] G. C. Strinati, P. Pieri, G. Ropke, P. Schuck, and M. Urban, *Physics Reports* **738**, 1 (2018), the BCS - BEC crossover: From ultra-cold Fermi gases to nuclear systems.
 - [17] S. Lerer, N. Bachar, G. Deutscher, and Y. Dagan, *Physical Review B* **90**, 214521 (2014).